Iranian Journal of Science and Technology, Transactions of Civil Engineering (2023) 47:3591–3608
https://doi.org/10.1007/s40996-023-01197-5

RESEARCH PAPER

Study on the Interaction Between Blasting Stress Waves with Different Incidence Angles and Crack

Huizhen Liu[1] · Liyun Yang[1] · Cheng Chen[2] · Renshu Yang[2]

Received: 27 September 2022 / Accepted: 2 July 2023 / Published online: 27 July 2023

Abstract

To better study rock blasting in engineering and the initiation and propagation behavior of the pre-existing crack under blasting stress waves, large-scale rock models containing a thorough centric crack were numerically blasted, using the LS-DYNA and HYPERMESH software for solving, modeling and meshing as well as adding keywords, respectively. The rock material chosen for the present study was granite, and the Holmquist–Johnson–Cook (HJC) model was applied to carry out numerical simulations. To study the influence of incident angle of blasting stress wave, there were four groups of modes in all designed with different borehole positions, labeled as M-1, M-2, M-3 and M-4. Based on the theoretical wavefront reconstruction, the reflection and diffraction of blasting-induced waves at a finite crack and highly complex interaction with crack were explained in detail. Furthermore, the maximum circumferential stress criterion was used to analyze the crack initiation and propagation. The results are in accordance with the experiment results, which show that the incident angles of blasting stress waves have a significant effect on the propagation characteristics of waves at the pre-existing crack and the model failure modes. As the incident angle increases, the initiating time of crack tip B decreases, but the deflecting angle increases, and damage near the pre-existing crack is more serious. In addition, reflected and diffracted waves cause stress concentration at the crack tip, which plays a dominant role in crack initiation and propagation. While the pre-existing crack hinders stress wave propagation and reduces its amplitude and inhibits the formation and development of cracks around the borehole, thereby resulting in that the model damage is mainly concentrated at the crack ends and around the borehole, no obvious damage occurs in other areas.

Keywords Crack propagation · Incident angle of blasting stress wave · Theoretical wavefront reconstruction · Fracture mechanics · Numerical simulation

List of Symbols

ρ	Density
ρ_0	Reference density
V	Relative volume
D	Detonation speed
P_{cj}	Detonation pressure
A,B, R_1, R_2, ω	Basic parameters of equation of state
C_0~C_6	Coefficients of linear polynomial equation of state
E	Internal energy per unit volume
α	Included angle between the incident wave and crack surface
$\sigma_{\theta\theta}$	Circumferential stress at a certain position
σ_{rr}	Radial stress
σ_x, σ_y and τ_{xy}	X-stress, Y-stress and shear stress
θ	Polar angle
$\mathrm{P_rP}$	Reflected waves generated by P wave
$\mathrm{P_d^AP}$, $\mathrm{S_d^AP}$	Diffracted waves generated by P wave at the crack tip A
$\mathrm{P_d^BP}$, $\mathrm{S_d^BP}$	Diffracted waves generated by P wave at the crack tip B
V + P, V_P	Schmidt head waves
R + P, R_P	Rayleigh waves

✉ Liyun Yang
yangly@cumtb.edu.cn

[1] School of Mechanics and Civil Engineering, China University of Mining and Technology-Beijing, Beijing 100083, China

[2] School of Civil and Resource Engineering, University of Science and Technology Beijing, Beijing 100083, China

$P_d^BP_d^AP$, $S_d^BP_d^AP$	Secondary diffracted waves generated by P_d^AP and S_d^AP waves at the crack tip B
$V+P_d^AP$, $V\_P_d^AP$	Schmidt head waves generated by P_d^AP and S_d^AP waves

1 Introduction

In mining and tunnel engineering, the rock is often broken by blasting. The propagation of blasting stress wave and fracture caused by it are the important phenomena in engineering. After the explosive is detonated, resulting shock wave quickly attenuates into stress wave with the increasing propagation distance. It can be a cylindrical, spherical or plane wave, which plays an important role in rock crushing. However, there are usually a lot of defects in natural rock mass, such as bedding, joint, pore and crack, which have a significant impact on the blasting effect and stability of rock mass. Saharan et al. (Saharan et al. 2006) discussed the rock fracturing mechanism due to blasting dynamic loading detailedly, pointing out that blasting stress wave is the dominant force of rock fracture. Due to the instantaneous nature of the blasting process, it is necessary to use numerical method. The interaction between blasting stress wave and defects in rock mass plays a critical role in crack initiation, propagation and arrest, while the existence of cracks will affect the reflection, transmission and diffraction of blasting stress waves, which is an important subject of rock dynamics and its related disciplines, but this process still remains challenging. The action mechanism of blasting stress wave is not understood enough, resulting in serious damage of surrounding rock and increased disasters in blasting construction. Therefore, it is necessary and urgent for further research on it.

Stress wave and crack propagation in fracture mechanics are widely studied by photoelastic method and caustic method. In the early, Dally (Dally 1980) carried out dynamic photoelastic experiments to research the interaction between blasting stress waves and cracks and holes. Theocaris (Theocaris and Katsamanis 1978) studied crack dynamic behavior under impact loads by caustics experiments, and results show that tensile stress pulses rather than compressive stress pulses make the initial notch propagate. Rommanith et al. (Rossmanith and Shukla 1981a, 1981b) conducted a dynamic photoelastic experiment on specimens with the prefabricated cracks and discussed the interaction between blasting stress waves and static crack as well as running crack and then theoretically analyzed the reflection and diffraction of P and SV waves at the crack tip under normal incidence, oblique incidence and tangential incidence. The results show that blasting stress waves have a vital effect on the stress field at the crack tip. Smith (Smith 1971) studied the interaction between a static crack and an impinging dilatational wave using photoelastic experiment. Zhu (1988, 1993) studied the effect of blasting-induced stress wave on the direction and velocity of crack propagation using dynamic photoelastic experiment and analysis method. Yang et al. (Yang et al. 2019, 2018) studied the interaction between blasting-induced stress wave and static crack, and running crack in the same direction and reverse direction by dynamic caustics and photoelastic experiments, and analyzed the dynamic characteristics of crack tip. More recently, Li et al. (Li et al. 2021) studied the crack propagation behavior and stress distribution at the end of defects under blasting by caustics method and ANSYS/LS-DYNA simulation. Yue et al. (Yue et al. 2017; Qiu et al. 2019, 2021) derived the stress field expression of crack tip by the optical geometry principle of ray deflection and proposed the theory of distorted caustics pattern, which was applied to study the interaction between the blasting stress wave and pre-existing crack. Chen et al. (Chen et al. 2022) studied the interaction process between the oblique incident blasting stress wave and the prefabricated crack and stress field at the crack tip by the photoelastic and numerical methods.

Additionally, Zhu et al. (Hu et al. 2015) studied numerically the crack propagation behavior of blasting model with a crack by developing a mixed failure criterion. Wang et al. (Wang et al. 2018) used a laser to generate Rayleigh wave and then simulated it interacting with a subsurface crack. Fan et al. (2019) used the numerical manifold method (NMM) to study the crack and wave propagation on underground rock mass and analyzed effects of stress wave and existing crack on the stress field. Lalegname et al. (Lalegname and Sändig 2011) discussed the influence of plane elastic waves on a running crack based on theoretical derivation and numerical analysis. Chen and Sih (Chen and Sih , 1977) have studied the cracks and waves scattering in theory under impact loading. Harris (1980) used the Cagniard-de Hoop technique to invert the various transforms, calculating expressions for a semi-infinite crack. However, there are many mathematical difficulties for the finite crack problem. Zhao et al. (Zhao et al. 2003) considered the nonlinear deformation constitutive relation (BB model) of the joints and deduced the wave propagation equation for normally incident elastic P wave across the rock joints by combining the characteristic function method. Li et al. (Li and Ma 2010) deduced a wave propagation equation for a linear elastic rock joint in view of the conservation of momentum at the wave fronts and the displacement discontinuity method. In addition, wave propagation equation derived can be appropriate for nonlinear rock joints with no need for the complex Fourier and inverse Fourier transforms.

As can be seen from the above researches, numerical investigation in dynamic crack–wave interaction is rather limited to date, covering incidence, reflection, transmission,

diffraction and surface waves. A large number of studies focused on analysis of experimental phenomena. Compared with the theory and experiment, the numerical method is more intuitive; parameters can be adjusted at any time, very high efficiency. Therefore, the blasting analysis of rock mass has gradually adopted numerical analysis as the main method and experiment as the auxiliary method and reduced experiment to avoid wasting manpower and material resources(Jing and Hudson 2002; Jing 2003).

Due to the complexity of a variety of waves and interaction between the waves and cracks, the mechanism of stress waves on crack has not been clearly concluded. Thus, in this paper, the interaction between blasting-induced stress waves with different incidence angles and crack has been systematically studied using numerical method combined with theoretical analysis, which is mainly divided into two parts. The objective of the first part is to analyze the effect of the pre-existing crack on blasting stress wave propagation and explain how the reflected, diffracted, surface and Schmidt head waves are created combined with theoretical wavefront reconstruction. It has been shown that the position and shape of the blasting-induced wave continuously evolve with time and the order in which the wave components appear is dependent on the propagation velocity in the rock. The second part of the study discusses about crack initiation and propagation induced by dynamic wave propagation based on the maximum circumferential stress criterion. The simulation results agree well with the published experimental results (Rossmanith and Shukla 1981a; Chen et al. 2022) which is conducive to our deep understanding of the blasting-induced stress wave propagation and the interaction mechanism between blasting stress wave and crack, suggesting a broad reference for the further development of rock blasting in engineering practice. It is worth noting that the pre-existing crack is the finite straight crack, and the incident P wave is considered in this study.

2 Theoretical Analysis

2.1 Generation of Stress Waves

Wave is any disturbance propagating in space or matter, which can be produced by dynamic loading, such as blasting, earthquake and impacting, and can be divided into the body wave and surface wave. They are the longitudinal wave (P wave) and the distortional wave (S wave) as well as Rayleigh wave (R wave), respectively. The longitudinal wave propagates in the parallel direction to the particle motion, while the distortional wave propagates in the perpendicular direction. The propagation of various waves generated by typical disturbances is shown in Fig. 1, which belongs to the spherical wave emission, with displacement amplitudes attenuating with radial distance. The propagation of two-dimensional stress waves is similar to it, such as explosive excitation generates P wave, S wave and R wave radiations. Figure 1b shows the numerical result of the waves generated by explosion excitation in a PMMA sample with free boundary conditions. The P wave, S wave, head wave and R wave have been explicitly predicted, which is consistent with Fig. 1a, indicating that numerical simulation can well characterize the wave propagation process and displacement field evolution. However, discontinuities, such as cracks, joints and large-scale faults, exist in natural rock masses, make the wave propagation and stress field changed. The reflection occurs on the crack surface and diffraction at the crack tip,

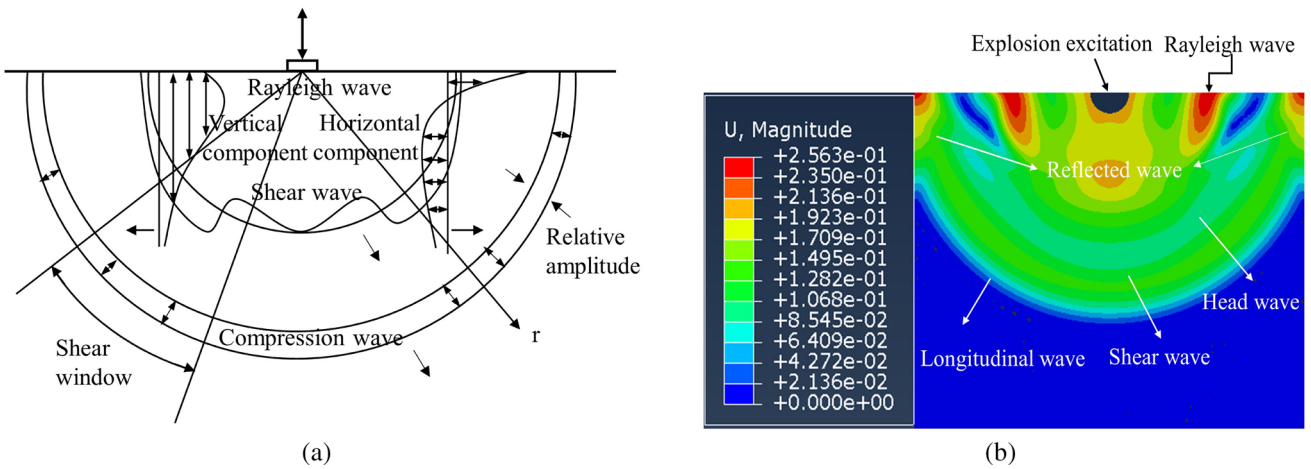

Fig. 1 **a** Displacement distribution in P wave, S wave and R waves (Woods 1968); **b** normal displacement fields of waves emission during explosion excitation

leading to stress concentration and even crack instability, and the crack will hinder the propagation of stress wave, which is a complex interaction process.

2.2 Establishment of Theoretical Analysis Model

To analyze the interaction between blasting stress waves with different incidence angles and crack, a theoretical analysis model is set up as illustrated in Fig. 2. Excited by blasting, P wave front divides the whole region into two parts: the disturbed area and undisturbed area. The included angle between the incident wave and the crack surface is α, $0^0 \le \alpha \le 90^0$. When the incident wave encounters the crack, it will be reflected on the crack surface to form a reflected tensile wave, and when the incident wave reaches crack tip, diffraction will occur to generate a diffraction wave.

The incident wave can be either a P wave or S wave. For the convenience of analysis, only the influences of P waves are considered with ignoring S wave in whole process. The incident wave is reflected on crack surface and diffracted at the crack tip, producing a total stress field $\sigma_{ij}(x, y, t)$; it may be considered as the simple superposition of the stress fields induced by incident wave and wave scattering about the crack. The diffraction and reflection wave stress fields are also called scattering wave stress fields; the incident wave and scattering wave stress fields are, respectively, written as $\sigma_{ij}^{(i)}(x, y, t)$ and $\sigma_{ij}^{(s)}(x, y, t)$. Therefore, stress state under the interaction between blasting stress wave and crack can be expressed as follows:

$$\sigma_{ij}(x, y, t) = \sigma_{ij}^{(i)}(x, y, t) + \sigma_{ij}^{(s)}(x, y, t) \tag{1}$$

and

$$\text{when } \left(x^2+y^2\right)^{\frac{1}{2}} \to 0, \sigma_{ij}^{(s)} \to 0$$

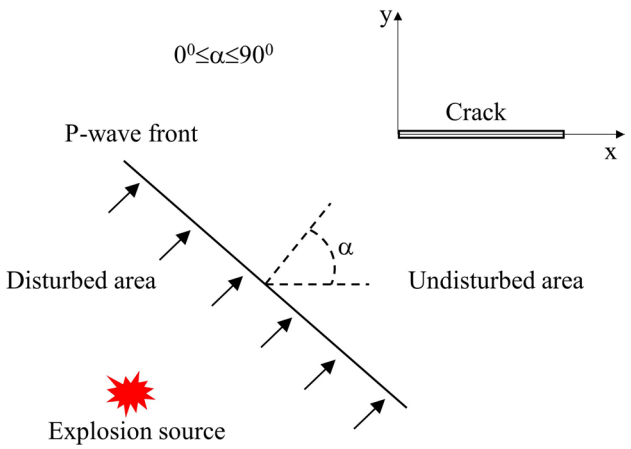

Fig. 2 Theoretical analysis model

3 Numerical Modeling and Material Parameters

Finite element method (FEM) has been generally applied in simulating rock blasting, which can provide the full-field data of blasting and obtain a better insight into the highly complex interaction process between stress wave and crack. Thus, in this study, the commercial finite element code LS-DYNA will be employed for solving, HYPERMESH software for modeling and meshing as well as adding keywords, LS-PREPOST for post-processing. The calculation termination time is 1000 μs, and the time step is set to 1 μs. The adopted system of unit is cm-g-μs in this section.

3.1 Model design

The paper adopts the large-scale model, and the rock material is the granite. A cuboid rock model with the length and width of 250 cm and height of 1 cm was modeled, having a 10-cm-diameter borehole and a thorough centric crack in the model. The charge mode is decoupled charge with decoupled coefficient being 2. The explosive is 5 cm in diameter, and the length and width of centric crack are $l = 100$ cm and $w = 0.5$ cm, respectively. In addition, r is the shortest distance from borehole to the crack, 50 cm. Incidence angle α of blasting stress wave is variable, $0^0 \le \alpha \le 90^0$. Based on the above analysis, by changing the borehole position in the model, that is, the incident angle of the blasting stress wave, the model was established. Meanwhile, to comprehensively and systematically analyze the interaction process between blasting stress waves with different incidence angles and crack and also reduce the workload, four representative models were established, with incident angles being 0°, 45° and 90°, respectively, and were marked as models M-1, M-2, M-3 and M-4, as shown in Fig. 3.

3.2 Establishment of Numerical Model

3.2.1 Element and the Selection of Algorithm

The solid 164 element is applied to the rock, explosive and air. Rock adopts the Lagrange algorithm. As the air and explosive deform greatly in the process of blasting, arbitrary Lagrangian–Eulerian (ALE) algorithm is utilized for the explosive and air, which avoids the numerical calculation difficulties caused by serious distortion and achieves the dynamic analysis of fluid–structure coupling. Air and explosive are bound in an element algorithm by

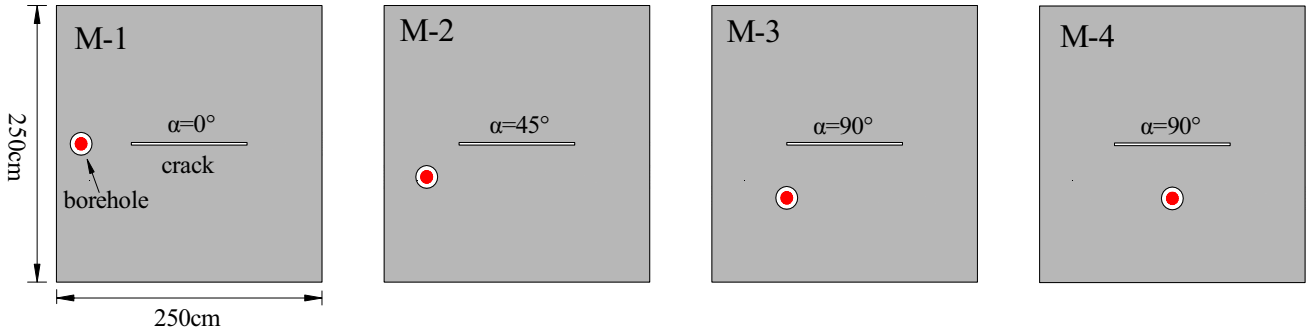

Fig. 3 Schematic diagram of blasting models with a thorough centric crack

Table 1 The HJC constitutive parameter of granite (Bi , 2018)

Parameter	ρ/kg·m^{-3}	f_c/MPa	A	B	C	S_{max}	G/GPa	T/MPa	D_1	D_2
Value	2600	154	0.28	2.5	0.00186	5	28.7	0.28	0.04	1.0
Parameter	P_{crush}/MPa	μ_{crush}	P_{lock}/ GPa	μ_{lock}	K_1/GPa	K_2/GPa	K_3/GPa	EF_{min}	N	FS
Value	51	0.00162	1.2	0.012	12	25	42	0.01	0.79	0.035

Table 2 The relevant parameters of the explosive (Wang , 2003)

Parameter	ρ/kg·m^{-3}	D/m·s^{-1}	P_{cj}/GPa	A /GPa	B /GPa	R_1	R_2	ω	E_0 /GJ·m^{-3}	V_0
Value	1500	7450	22	625.3	23.29	5.25	1.6	0.28	8.56	1.0

Table 3 The relevant parameters of air (Gao and Wu 2015)

Parameter	ρ/kg·m^{-3}	C_0/ GPa	C_1	C_2	C_3	C_4	C_5	C_6	E_0 /MJ·m^{-3}	V_0
Value	1.290	0	0	0	0	0.4	0.4	0	0.25	1.0

*ALE_MULTI_ MATERIAL_GROUPA keyword. In addition, in modeling, it is necessary to separate grids for explosive and air and give their own equations of state.

3.2.2 Material Parameters and the Equation of State

To model the rock material with a crack, the rock is modeled with the HJC (Holmquist–Johnson–Cook) material model. In this paper, *MAT_ADD_EROSION failure criterion is introduced to control element failure and principal stress criterion is set, i.e., when the stress and strain are set in the finite element model, the element exceeding the set value will be deleted and then cracks are formed in the model. The parameters of granite material are shown in Table 1.

To calculate the detonation products, explosives need to be defined by the keyword *MAT_HIGH_EXPLOSIVE_BURN in conjunction with the John–Wilkins–Lee (JWL) equation of state. The JWL equation expressed in terms of the pressure of detonation product:

$$P = A\left(1 - \frac{\omega}{R_1 V}\right)e^{-R_1 V} + B\left(1 - \frac{\omega}{R_2 V}\right)e^{-R_2 V} + \frac{\omega E}{V} \quad (2)$$

where P is pressure generated by the explosion; V is the relative volume; E is the internal energy per unit volume and A, B, R_1, R_2 and ω are basic parameters. The relevant parameters are presented in Table 2, ρ represents density of explosive, D represents detonation speed, and P_{cj} represents detonation pressure.

The air medium was considered, which was added by the keyword *MAT_NULL. Linear polynomial equation of state was adopted for air and was defined by the keyword *EOS_LINEAR_PLOYNOMIAL and can be expressed as follows:

$$P = \left(C_0 + C_1\mu + C_2\mu^2 + C_3\mu^3\right) + \left(C_4 + C_5\mu + C_6\mu^2\right)E \quad (3)$$

where C_0~C_6 are coefficients of equation of state; P is the detonation pressure; E is the internal energy per unit volume;

$\mu = \rho / \rho_0 - 1$,ρ is the density of air, and ρ_0 is the reference density. The relevant parameters are displayed in Table 3.

3.2.3 Modeling

The finite element model was established by HYPERMESH software, which mainly consists of three parts: air, explosive and rock. Single-layer solid grid was used to mesh the model, and the total number of elements is more than 128,408. Time step was set as 1 μs, and maximum mesh size is not more than 1 cm. The explosive grid and the air grid are shared nodes at the interface. Under blasting stress wave, the rock deformation may occur, leading two interfaces of the crack along its length to contact each other. Therefore, automatic surface to surface contact was set up at both interfaces. In the meantime, to better compare and analyze, the area near the borehole in all models has the same meshing, and Fig. 4 illustrates the details of the part mesh of model in HYPERMESH.

In dynamic analysis, the stress waves are reflected from the boundaries of the model and converted into tensile waves, which will cause rock fragments. Therefore, to more realistically simulate the propagation of waves through rock mass, absorbing boundaries were employed in all sides with the exception of pre-existing crack boundaries, which are the free faces by the keyword *BOUNDARY_NON_REFLEC-TION, so that no reflection waves will be generated when the blasting stress waves arrive at the model boundaries. A normal constraint was imposed in the thickness direction of model.

4 Results and Analysis

4.1 Influence of the Pre-existing Crack on Blasting Stress Wave Propagation

After the explosive detonation, the cylindrical P wave radiates outward from the explosion source. When it propagates for a certain distance, which can be considered as a plane P wave (Li et al. 2018). Stress concentration around crack tips results in the cracking of rock mass and further affects stress wave propagation. Propagation characteristics of the wave will vary along the crack when the incident wave comes from different directions, as shown sequence of pictures in Figs. 5, 7, 10 and 12. It can be clearly seen that the position and shape of the blasting-generated waves continuously evolve with time, through which the interaction between blasting stress waves from different directions and crack can be analyzed intuitively. Nevertheless, the latter wave system has not been given here because of the limited space in the paper, and it is not so significant for analysis when that attenuates to a certain extent.

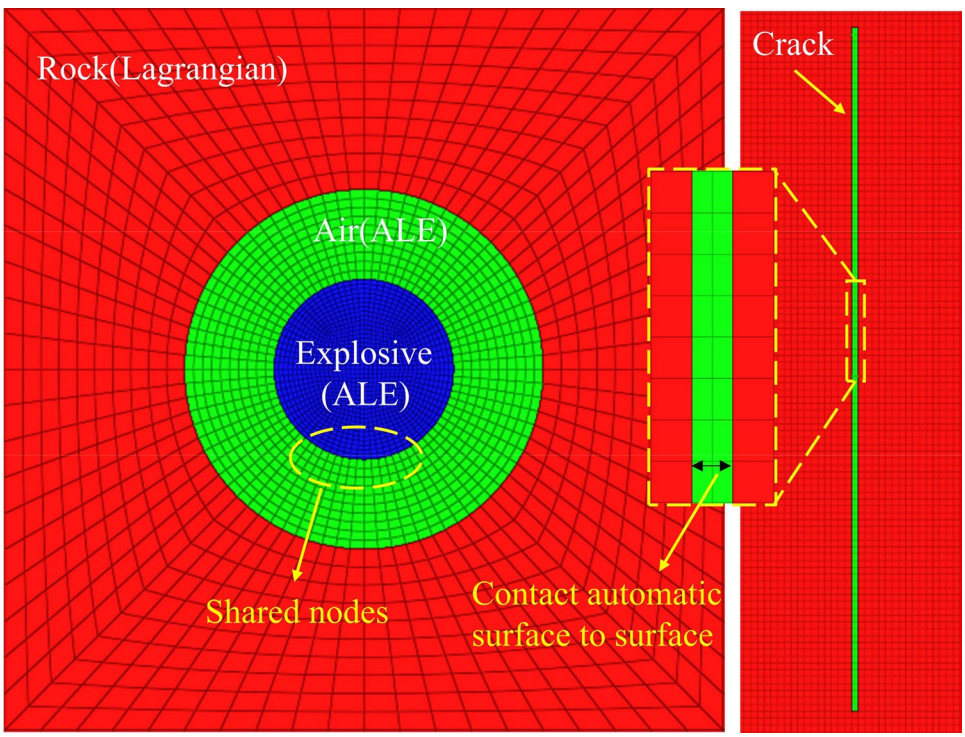

Fig. 4 The part mesh of model

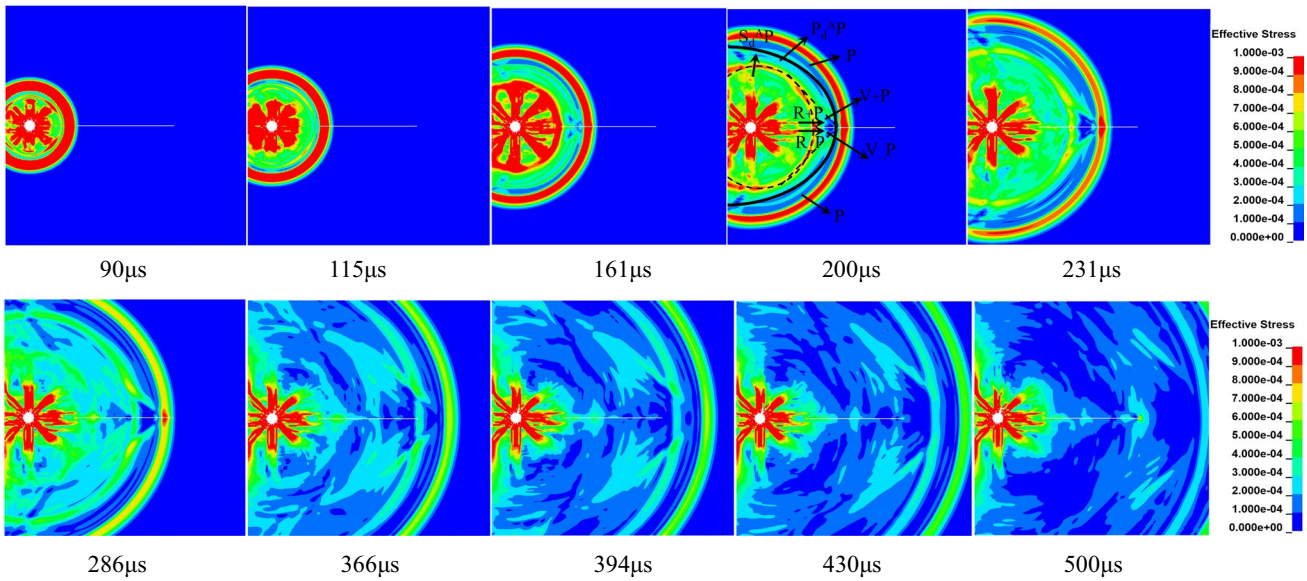

Fig. 5 Propagation process of the blasting-generated waves at the crack in the model M-1

4.1.1 Incident Angle 0°

(1) Model M-1

For model M-1, the direction of wave propagation is parallel to the crack line, i.e., the stress wave front is vertical to the crack walls. Figure 5 shows the effective stress contours of interaction between blasting stress wave and crack at different times in the model as a result of the explosive detonation. First of all, the blasting stress wave radiates outward from the explosion source position. Before the blasting stress wave interacts with crack, and it propagates to the right and approaches the crack tip continuously, corresponding contour is not presented in Fig. 5. As can be seen from the sequence figures, when $t = 90$ μs, the stress wave arrives at left tip A of the crack. After that, the blasting stress wave begins to interact with crack. Wave diffraction occurs at tip A and reflection on the upper and lower surfaces of the crack, which lasts until the stress wave propagates to the right tip B of the crack.

Based on blasting simulation results, P wave diffraction at the crack tip A is displayed at $t = 200$ μs, and associated wavefront reconstruction is displayed in Fig. 6, where the superscript "+" in Fig. 6 represents the upper surface and "-" denotes the lower surface. When the P wave is diffracted at the crack tip A, both P_d^AP wave and S_d^AP wave are generated. During wave propagation, the P wave is reflected at the surfaces of the crack to generate the so-called Schmidt head waves (V + P, V_P), which are tangent to the diffracted S_d^AP wave (Yue et al. 2019). However, there are no reflected P_rP wave and S_rP wave produced in this case. At the same time, Rayleigh waves R + P and R_P are formed on the upper and lower surfaces of the crack and propagate from tip A to tip B along the crack walls. These waves (Hoop 1958) gradually travel to the right and attenuate.

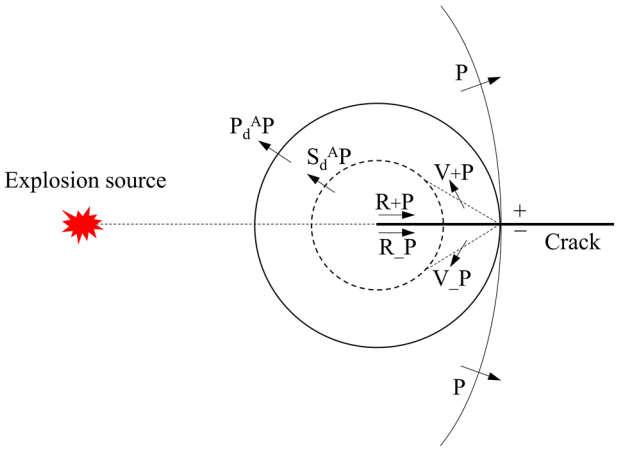

Fig. 6 Schematic of the theoretically generated wavefront construction in the model M-1

4.1.2 Incident Angle 45°

(1) Model M-2

For model M-2, P wave impacts on the crack tip at an angle of 45 deg with respect to the crack surface; Fig. 7 shows wave propagation at different time steps. When P

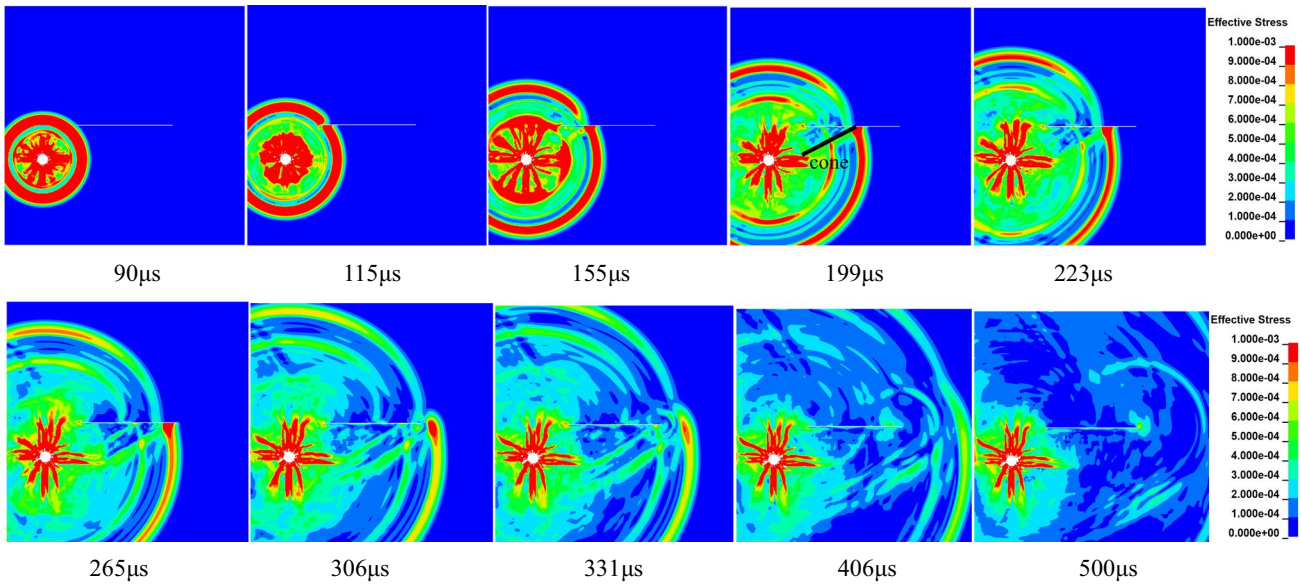

Fig. 7 Propagation process of the blasting-generated waves at the crack in the model M-2

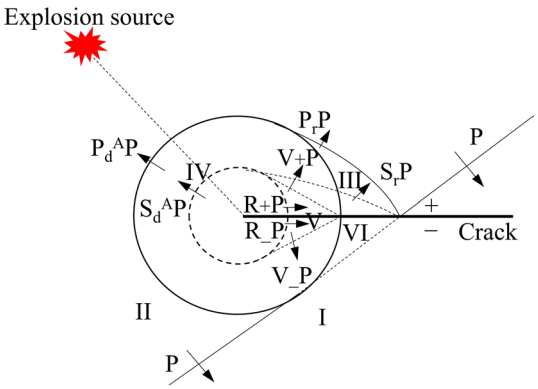

Fig. 8 Schematic of the theoretically generated wavefront construction in the model M-2

wave obliquely impinges on a static crack, the diffraction and reflection will occur. In the same way, it can be seen that the blasting stress wave propagates freely and approaches the crack continuously before $t = 90$ μs from Fig. 7. When $t = 90$ μs, blasting stress wave moves to the left tip A of crack; it then begins to interact with the crack. During the interaction between wave and crack, the field near the crack tip is disturbed, but disturbance does not occur in the far field. Thus, undisturbed area I and disturbed area II can be identified, and disturbed area II is the main action region, including reflection area III, diffraction area IV, Schmidt head wave area V and shadow area VI, as shown in Fig. 8. Figure 8 shows the theoretically generated wavefront reconstruction due to blasting load. P wave propagates to lower

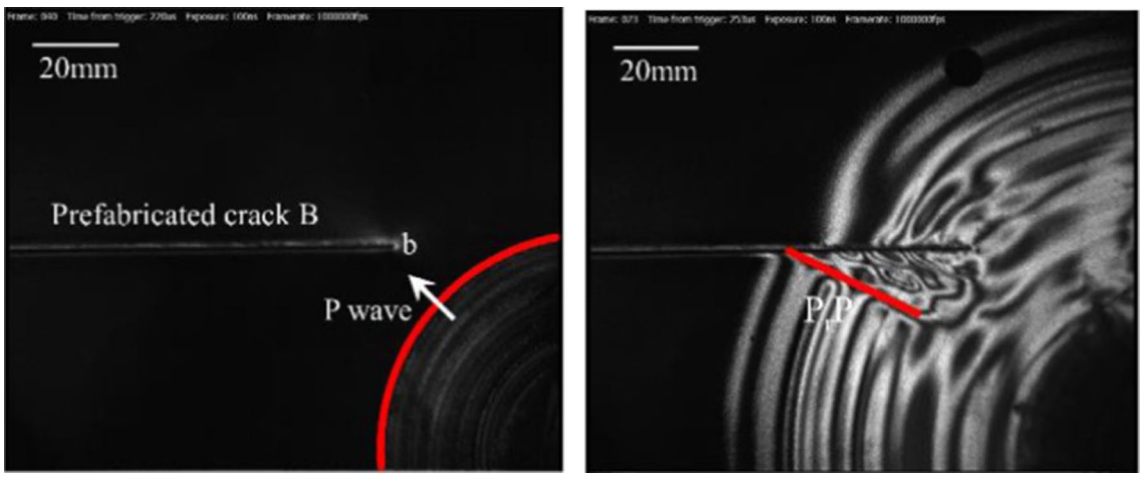

Fig. 9 Propagation of blasting stress wave in the experiment (Chen et al. 2022)

surface of the crack, generating reflected P_rP wave and SrP wave. Note that, $t = 199$ μs, a clear boundary cone has been made at the interface between the reflected P_rP wave and P wave, which is consistent with the experimental results (Chen et al. 2022), as displayed in Fig. 9. The P wave is diffracted at the crack tip A; both $P_d{}^AP$ and $S_d{}^AP$ waves have been generated. In addition, producing the so-called Schmidt head waves V + P and V_P, which are tangent to the diffracted $S_d{}^AP$ wave, Rayleigh waves R + P and R_P are formed on crack surfaces and travel along the crack walls from tip A to tip B. As the waves gradually propagate to the right, diffraction also starts to occur at tip B, inducing diffracted $P_d{}^BP$ wave and $S_d{}^BP$ wave, which can be seen from the subsequent figures in Fig. 7. And $t = 331$ μs, the diffraction waves at crack tips A and B are joined together. The process will be described in detail later, in the mode M-3.

4.1.3 Incident angle 90°

(1) Model M-3

In fact, the model M-3 is similar to model M-2. In this case, P wave is vertically incident on the crack surface. The reflection and diffraction of a P wave about the crack are shown in Fig. 10, and the associated theoretical results are shown in

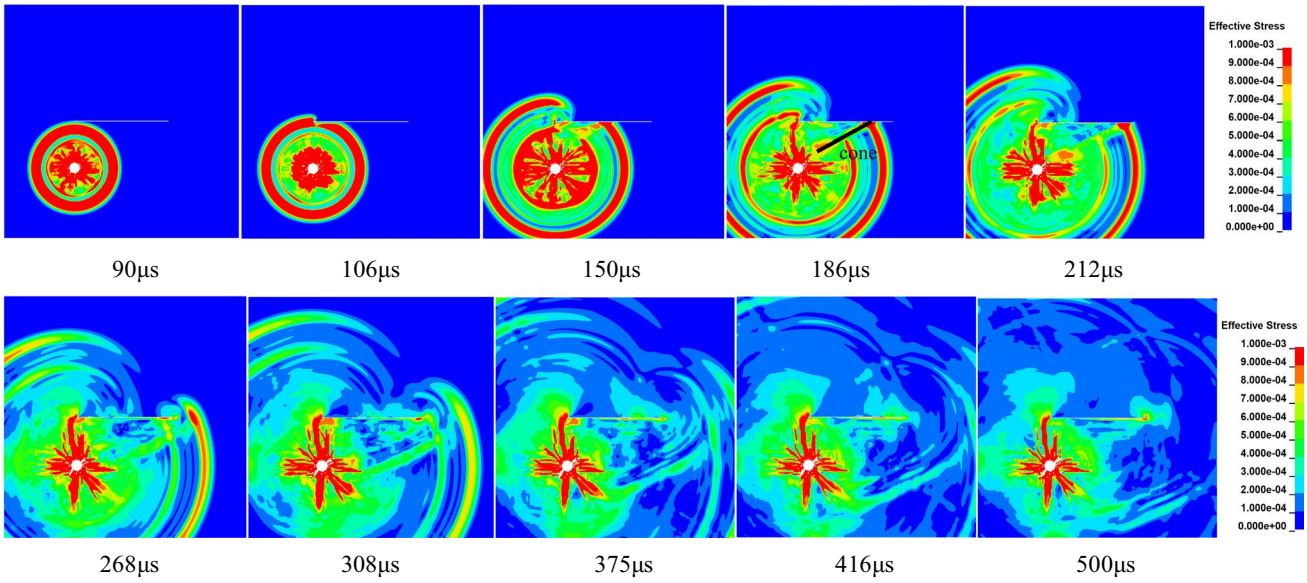

Fig. 10 Propagation process of the blasting-generated waves at the crack in the model M-3

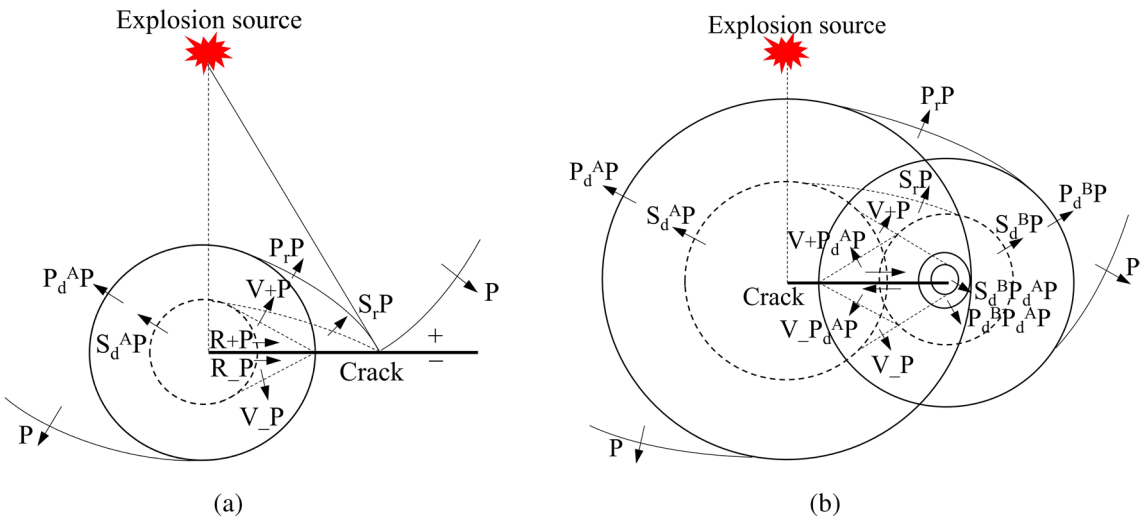

Fig. 11 Schematic of the theoretically generated wavefront construction in the model M-3

Fig. 11a, b, respectively. Similarly, the blasting stress wave propagates freely and approaches the crack tip continuously in the early stage, and by the time the interaction occurs, corresponding contour is not given in Fig. 10. As can be seen from the sequence figures, when $t = 90$ μs, the stress wave extends to crack lower surface. After that, it begins to interact with the crack, and the crack hinders the stress wave propagation. When the stress wave arrives at the left tip A of the crack, diffraction occurs at tip A and reflection occurs on crack lower surface, which lasts until the stress wave propagates to the right tip B of the crack. At $t = 150$ μs, P wave is diffracted at the crack tip A; both $P_d{}^AP$ wave and $S_d{}^AP$ wave are formed. During the propagation phase, the P wave is reflected at the lower surface of the crack to generate reflected PrP wave and S_rP wave. In the same way, a clear boundary cone is visible at the interface between the reflected P_rP wave and P wave. In addition, producing so-called Schmidt head waves (V + P, V_P), which are tangent to the diffracted $S_d{}^AP$ wave, Rayleigh waves R + P and R_P are formed on crack surfaces and travel along the crack walls from tip A to tip B. During this period, the interaction between P wave and crack and the corresponding wavefront reconstruction are shown in Fig. 11a. As the waves gradually propagate to the right, in the subsequent figures, the wave system becomes extremely complicated. When the stress wave propagates to the crack tip B, diffraction also occurs at tip B, inducing diffracted $P_d{}^BP$ wave and $S_d{}^BP$ wave. Different from the crack tip A, except for diffracted $P_d{}^BP$ wave and $S_d{}^BP$ wave, reflected P_rP wave and S_rP wave, Rayleigh waves R + P and R_P and Schmidt head waves V + P and V_P, the $P_d{}^AP$ and $S_d{}^AP$ waves formed by diffraction at the crack tip A have secondary diffraction at the crack tip B, inducing diffracted $P_d{}^BP_d{}^AP$ and $S_d{}^BP_d{}^AP$ waves. And $S_d{}^BP_d{}^AP$ wave is tangent to the produced Schmidt head waves $V + P_d{}^AP$ and $V\_P_d{}^AP$. The interaction process and theoretical wavefront reconstruction are shown in Fig. 11b. Moreover, $t = 375$ μs, the diffraction waves at crack tips A and B hold hand with each other, then fuse together and propagate to the right; they gradually attenuate and dissipate, eventually.

(2) Model M-4

Different from the above three models, models M-1, M-2 and M-3, the explosion source of model 4 is located directly below the midpoint of the crack, and generating the blasting stress wave after detonation impinges vertically on the crack surface. Figure 12 shows the interaction process; it is observed that the graphics are symmetrical with respect to the connection line between the midpoint of the crack and borehole at the different times. The propagation of blasting stress wave is the same as that in the early stage in the mode M-1, M-2 and M-3, which is all freely propagated. At $t = 90$ μs, the P wave front reaches the lower surface of crack. After $t = 90$ μs, P wave has a very complex interaction with crack. When $t = 106$ μs, the P wave extends to the tip A and tip B of crack. In the meantime, reflected waves P_rP and S_rP are induced and can be seen clearly at $t = 133$ μs. The experimentally recorded isochromatic fringe patterns of blasting stress wave with a crack in Fig. 13 show an apparent reflection phenomenon from the surface of crack (Chen et al. 2022). At $t = 213$ μs, the diffracted $P_d{}^AP$ wave, $S_d{}^AP$ and diffracted $P_d{}^BP$, $S_d{}^BP$ wave have been induced due to P wave interacting with the crack tip A and tip B, and as the waves propagate little by little, the graphic likes an "apple"

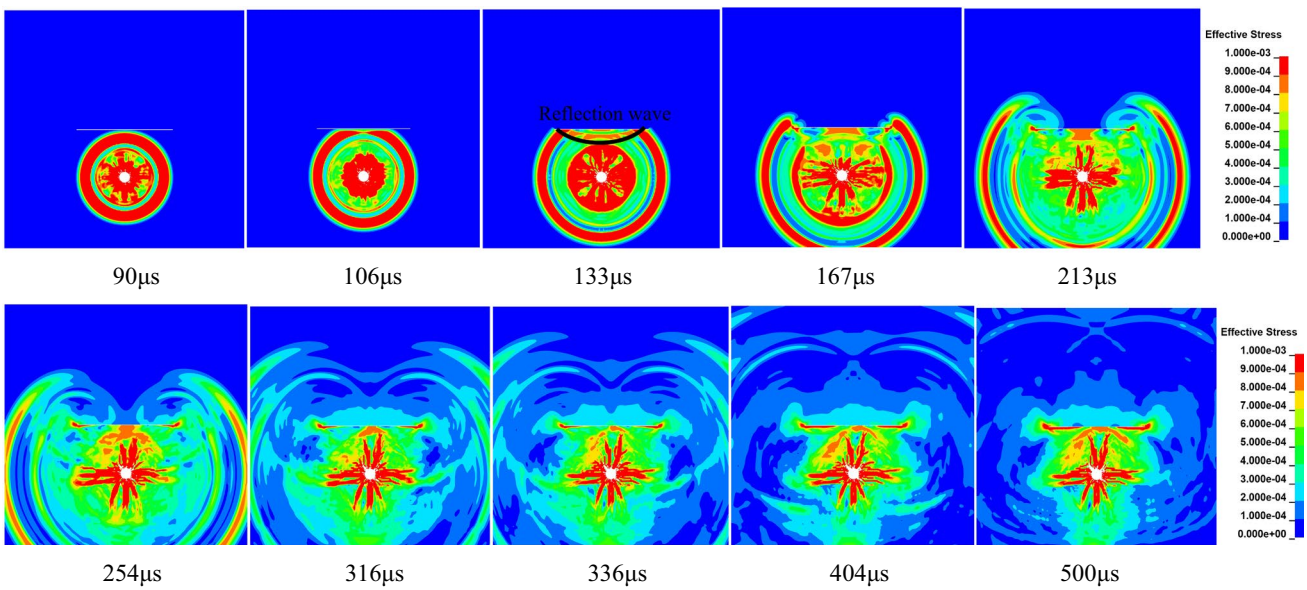

Fig. 12 Propagation process of the blasting-generated waves at the crack in the model M-4

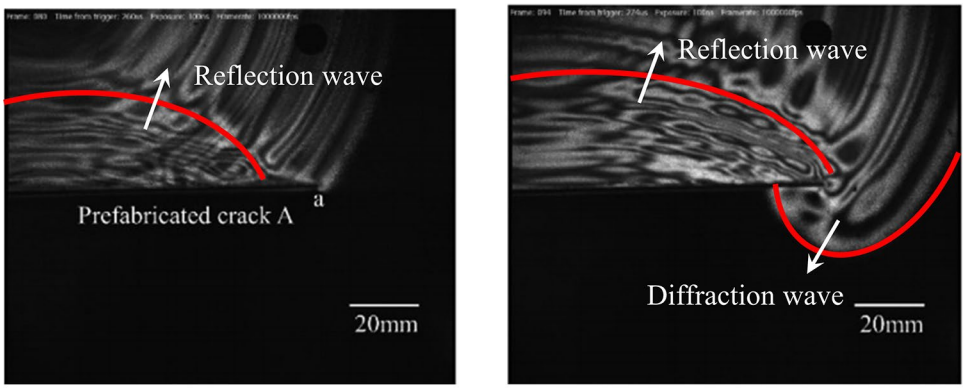

Fig. 13 Isochromatic fringe patterns of blasting stress wave propagation in the experiment (Chen et al. 2022)

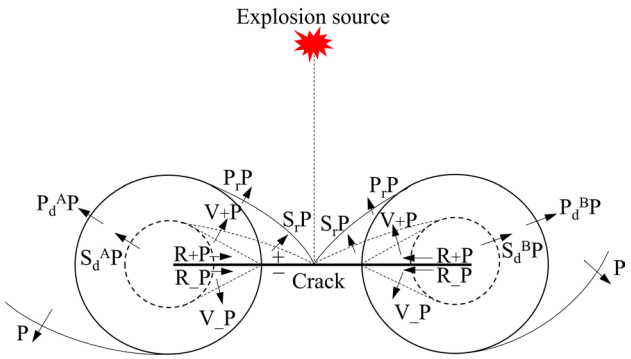

Fig. 14 Schematic of the theoretically generated wavefront construction in the model M-4

at $t = 254$ μs. The numerical results of P wave reflected on the crack surface and diffracted at the crack tip are in agreement with the results of photoelastic experiment (Chen et al. 2022), as shown in 14(b). With the Schmidt head waves V + P and V_P and Rayleigh waves R + P and R_P, the theoretical wavefront reconstruction is presented in Fig. 14a.

It should be pointed out that crack initiation time varies with stress wave incidence angles, which will be discussed later. Furthermore, as the stress waves continue to propagate, the energy attenuates quickly.

4.2 Crack Initiation and Propagation

As described in Sect. 2, the diffraction process of the blasting stress wave with different incident angles at the crack tip produces high local stress, which may lead to unstable crack propagation. The photoelastic experiments have also proved that the stress wave makes crack initiate and propagate (Dally et al. 1975). Figure 15a–d displays the failure modes of the models M-1, M-2, M-3 and M-4 with time after detonation, in angular degree range 0^0–90^0. To analyze the failure modes combination with the stress states (tension and compression) during the propagation of blasting stress wave, Fig. 16a–d shows the pressure evolution curves with time at a certain point when the incident angle $\alpha = 0°$, 45° and 90°; the pressure change of four measuring points is presented, where positive value denotes compressive; negative value represents tensile. The measuring points a1, a2, a3 and a4 are set in M-1 as displayed in Fig. 15a ($t = 100$ μs), which are located at the crack tip, the midpoint of the upper and lower surfaces of the crack, respectively, and a3 and a4 are symmetrical about the crack surface. Moreover, the measuring points b1, b2, b3 and b4 in M-2, c1, c2, c3 and c4 in M-3 and d1, d2, d3 and d4 in M-4 are also presented in Fig. 15, which is the same as that in the model M-1.

4.2.1 Failure Modes of Model

As shown in Fig. 15, the fracture of the models is mainly concentrated at the pre-existing crack tip and around the borehole, while there is no obvious fracture in other areas. With the increase in the incident angles, the damage near the crack becomes more serious. In addition, the crack hinders the propagation of blasting stress wave, resulting in more energy dissipation, and also restricts the formation and development of cracks around the borehole. Except for the blasting-induced cracks, the stress concentration occurs at the crack tips, thus driving the crack to initiate at both ends. When the energy gathered at the end exceeds the fracture toughness, the crack initiation and propagation occur. It can be found that the crack tips A and B of the four models initiate and propagate, respectively. In the early stage of free propagation of blasting stress waves, the damage degree of models M-1, M-2, M-3 and M-4 is basically the same because it is not influenced by the pre-existing crack. After that, it propagates to the crack tip A and begins to interact with the crack; then, the crack tip A initiates and propagates. As the crack tip A is close to the borehole, the crack initiation occurs firstly and then is connected with the radial crack radiated from the borehole, but the propagation length is also

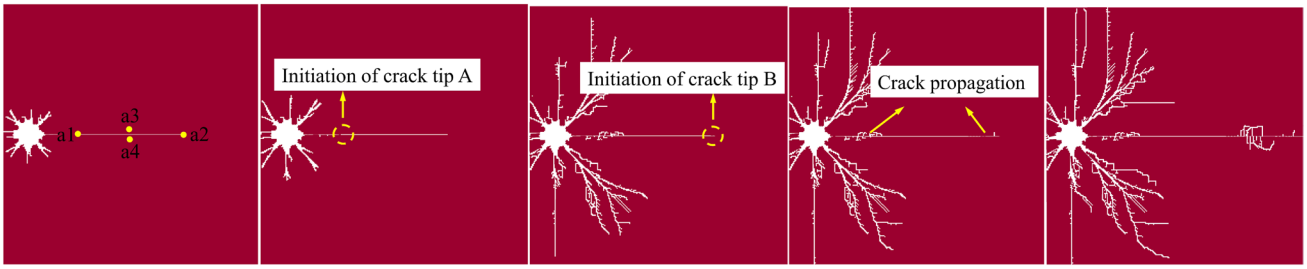

100μs 150μs 438μs 544μs 1000μs

(a) model M-1 (α=0°)

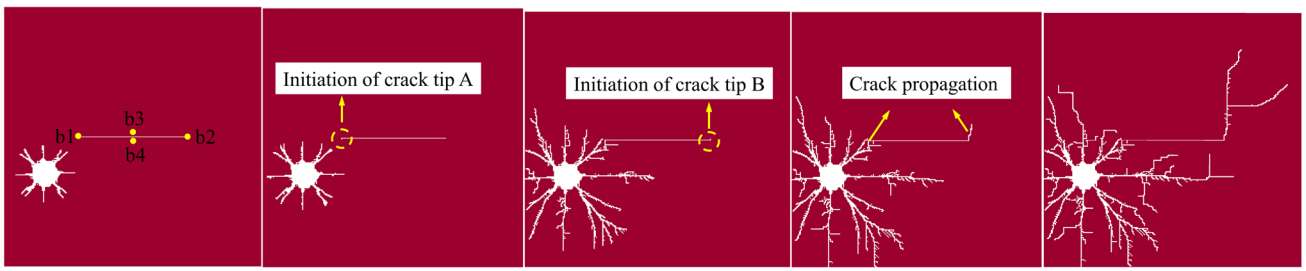

100μs 121μs 281μs 396μs 1000μs

(b) model M-2 (α=45°)

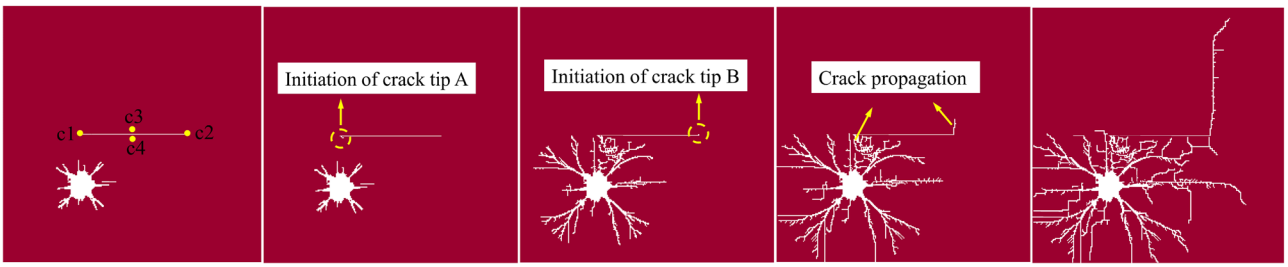

100μs 104μs 225μs 303μs 1000μs

(c) model M-3 (α=90°)

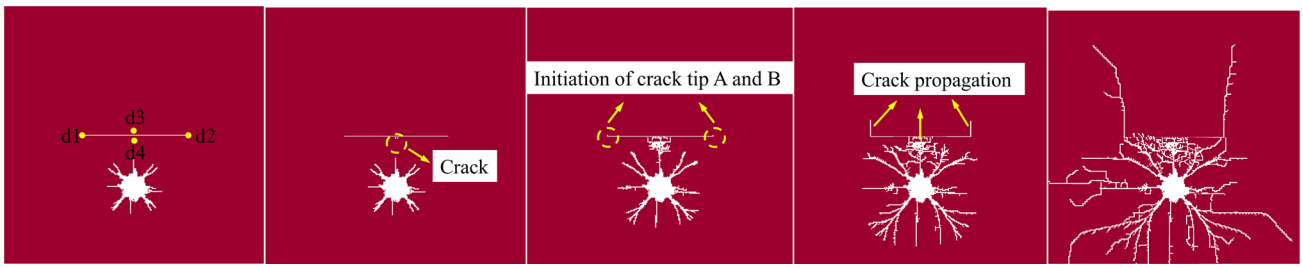

100μs 106μs 148μs 223μs 1000μs

(d) model M-4 (α=90°)

Fig. 15 The fractural forms of rock models with different incident angles of blasting stress wave

limited, in models M-1, M-2 and M-3. Only the crack tip A in the model M-4 can propagate to a certain length. The initiation times of the crack tip B in the models M-1, M-2, M-3 and M-4 are 438 μs, 281 μs, 225 μs and 148 μs, respectively. It can be found that the initiation time of crack tip B is obviously advanced, and the deflecting angle increases

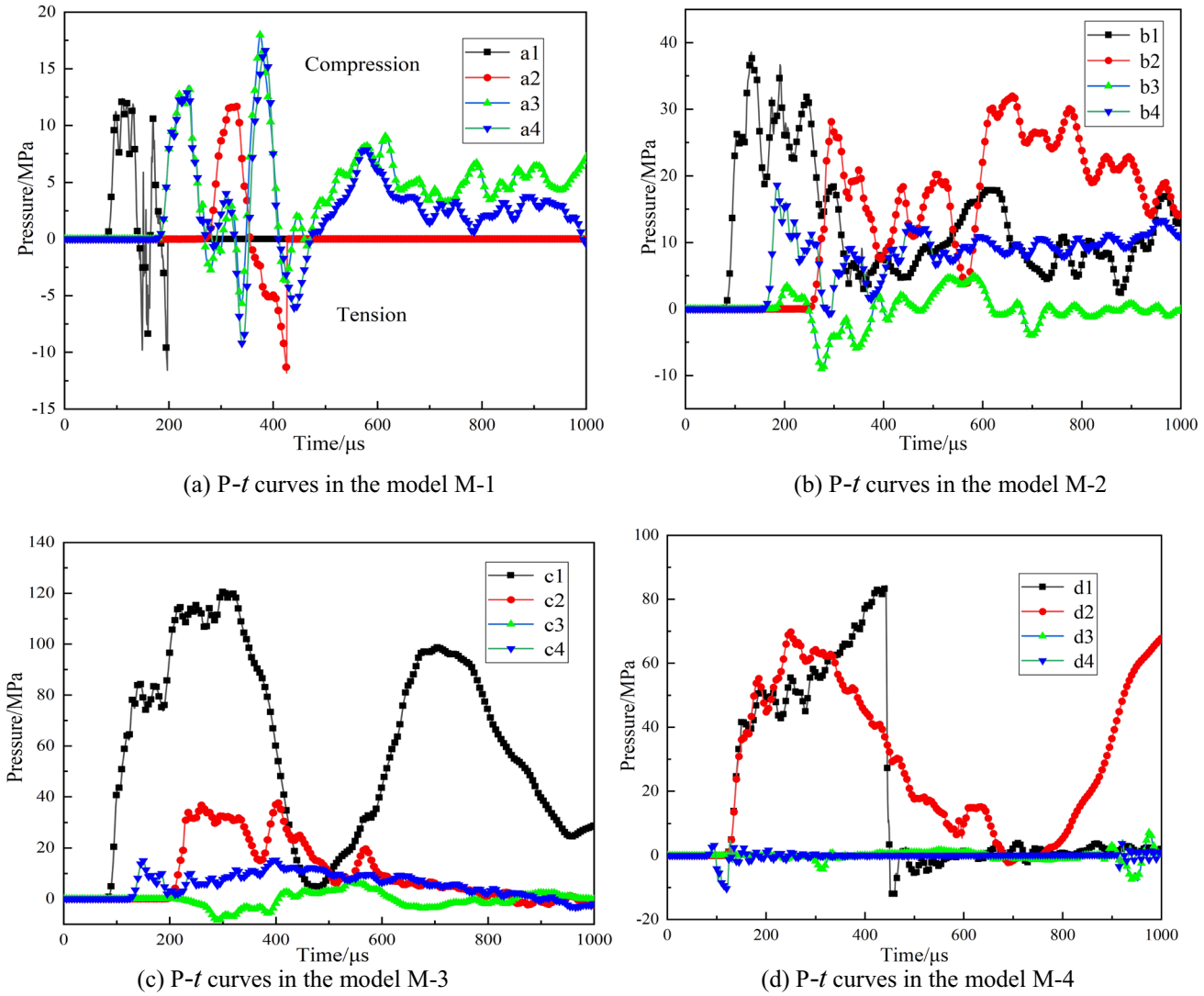

(a) P-*t* curves in the model M-1

(b) P-*t* curves in the model M-2

(c) P-*t* curves in the model M-3

(d) P-*t* curves in the model M-4

Fig. 16 The pressure–time curves of the measuring points in the four models

with the incident angle α increasing. In the model M-1, the crack tip B propagates to the right after initiation and then runs through the right boundary of the model. However, in the models M-2, M-3 and M-4, in the later stage of crack propagation, the blasting stress wave is basically dissipated. Although the crack continues to propagate by inertia, it does not penetrate through eventually and stops before reaching the model boundary. The pre-existing crack is symmetric about the borehole, following a path almost parallel to the crack surface in the model M-1, and the crack forms at crack tips A and B are basically consistent in the model M-4. It should be pointed out that a new crack appears at a certain distance from the lower surface of the pre-existing crack at first in the model M-4. Furthermore, compared with Figs. 5, 7, 10 and 12, it is also found that the crack initiation time is much greater than the time that the wave propagates from the explosion source to the crack tip A for four models. Thus, the incident wave, reflected wave and diffracted wave have an effect on crack initiation and propagation.

4.2.2 Pressure–Time History Curves

The incident angle of blasting stress wave influences the time of various stress waves arriving at the crack tip. Figure 16 displays the pressure–time curves on measuring points in the M-1, M-2, M-3 and M-4. Combined with the propagation process of blasting stress waves, the failure modes of the model shown in Fig. 15 will be analyzed in detail. The four models are different in terms of initiation and propagation of the pre-existing crack. As shown from Fig. 16, the curve at each measuring point goes up and down, which mainly is the action of compressive stress and tensile stress caused by blasting stress waves.

From Fig. 16a, it can be seen that, after blasting, the crack tips A and B (measuring points a1 and a2) are compressed first and then strained in the model M-1. The measuring point a1 is firstly influenced by blasting stress waves and point a2 last. As the pre-existing crack is symmetric with respect to the borehole, the trend of pressure at the a3 and a4 is the same on the whole. The crack tip A first initiates due to the tensile stress caused by the diffraction wave at $t = 150$ μs, and it gradually propagates to the left and then interconnects with the radial crack emanating from the borehole, as shown in Fig. 15a. At $t = 438$ μs, crack tip B initiates and then starts to propagate to the right, and it quickly reaches the right boundary of the model. This failure behavior in Fig. 16a presents the pressure at measuring points a1 and a2 changes to zero. Eventually, the fracture mode is formed, and the crack propagates to both ends along the horizontal direction approximately, and the propagation path does not change significantly.

As shown from Fig. 16b, crack tips A and B (measuring points b1 and b2) have been subjected to compressive stress. Similar to model M-1, blasting stress wave firstly acts on measuring point b1 and finally acts on the point b2 in the model M-2. The pressure evolution of the b3 and b4 is different, which is mainly because measuring point b4 is first subjected to compressive wave and then reflected wave from the lower surface of crack, while measuring point b3 is mainly subjected to diffraction wave. When $t = 121$ μs, crack tip A is affected by the diffraction wave and then attracted by the radial crack from the borehole, and initiates downward until propagating to intersect with the radial crack radiated from borehole. Measuring point b2 is first affected by compression wave and then diffraction wave. When $t = 281$ μs, the crack tip B begins to initiate upward and then bifurcates under the action of diffraction wave.

As displayed in Fig. 16c, it could be observed that the blasting stress wave arrives first at the measuring point c1 and measuring point c3 at last. Measuring point c1 is subjected to compression wave and diffraction wave, appearing two peak pressures, which peaks 120 MPa at 300 μs and 99 MPa at 715 μs, respectively. At $t = 104$ μs, the crack tip A initiates to the lower right and then is connected with the radial crack emanating from the borehole. No blasting wave is transmitted to the upper surface (measuring point c3), which is mainly affected by the tensile stress of diffraction wave at the crack tips A and B. The measuring point c4 is subjected to compression waves. Measuring point c2 is also subjected to compression wave and diffraction wave, which drives the crack tip B to initiate upward at $t = 225$ μs, and then propagates. Finally, the crack arrests due to the attenuation of blasting stress wave.

Figure 16d shows that the measuring point d4 is firstly influenced by the blasting stress waves and d3 at last, and point d4 is first compressed and then subjected to the action of the reflected tension wave. Since there is no blasting stress wave transmitted, the pressure on the upper surface of the crack (measurement point d3) is almost zero. After that, the diffracted waves of crack tips A and B have a weak effect on it. At $t = 106$ μs, a new crack appears at a certain distance from the lower surface of pre-existing crack; the reason is that the reflected tension waves from the lower surface of crack act on it. And it intersects with the radial crack radiated from borehole to form the crushing zone at last, in the model M-4, as shown in Fig. 15d. At $t = 148$ μs, crack tips A and B initiate and propagate upward successively. Note that, the pressure of the measuring point d2 rises again in the later stage; this is because the crack starting from crack tip A stops due to deflection and bifurcation, resulting in the energy accumulation at the crack tip B (measurement point d2).

4.2.3 Stress Field at the Crack Tip Induced by Blasting Stress Wave with Different Incidence Angles

In fracture mechanics, the attention is paid to the stress concentration near the crack tip. To further assess the above-mentioned issue, the maximum circumferential stress criterion was used to analyze the crack initiation and propagation behavior under blasting stress wave with different incidence angles. Meanwhile, in order to conveniently study the stress distribution of the pre-existing crack tip, Fig. 17 illustrates that the local coordinate system is set up with the midpoint of the crack as the origin. The literature (Herakovich 2016) gives the stress expression at a certain position near the crack tip, and it can be written as

$$\begin{cases} \sigma_{\theta\theta} = \sigma_x \cos^2\theta + \sigma_y \sin^2\theta - 2\tau_{xy} \sin\theta \cos\theta \\ \sigma_{rr} = \sigma_x \sin^2\theta + \sigma_y \cos^2\theta + 2\tau_{xy} \sin\theta \cos\theta \end{cases}$$

where $\sigma_{\theta\theta}$ represents the circumferential stress at a certain position; σ_{rr} represents corresponding radial stress; σ_x, σ_y

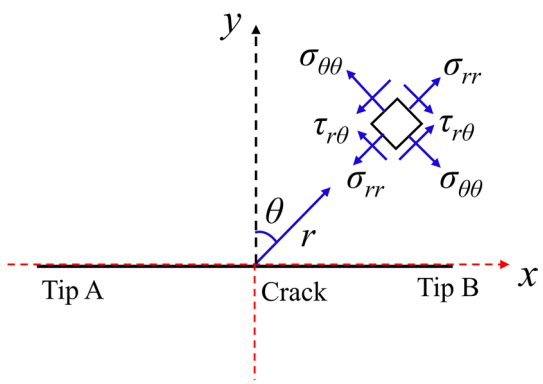

Fig. 17 Schematic of the created polar coordinate system

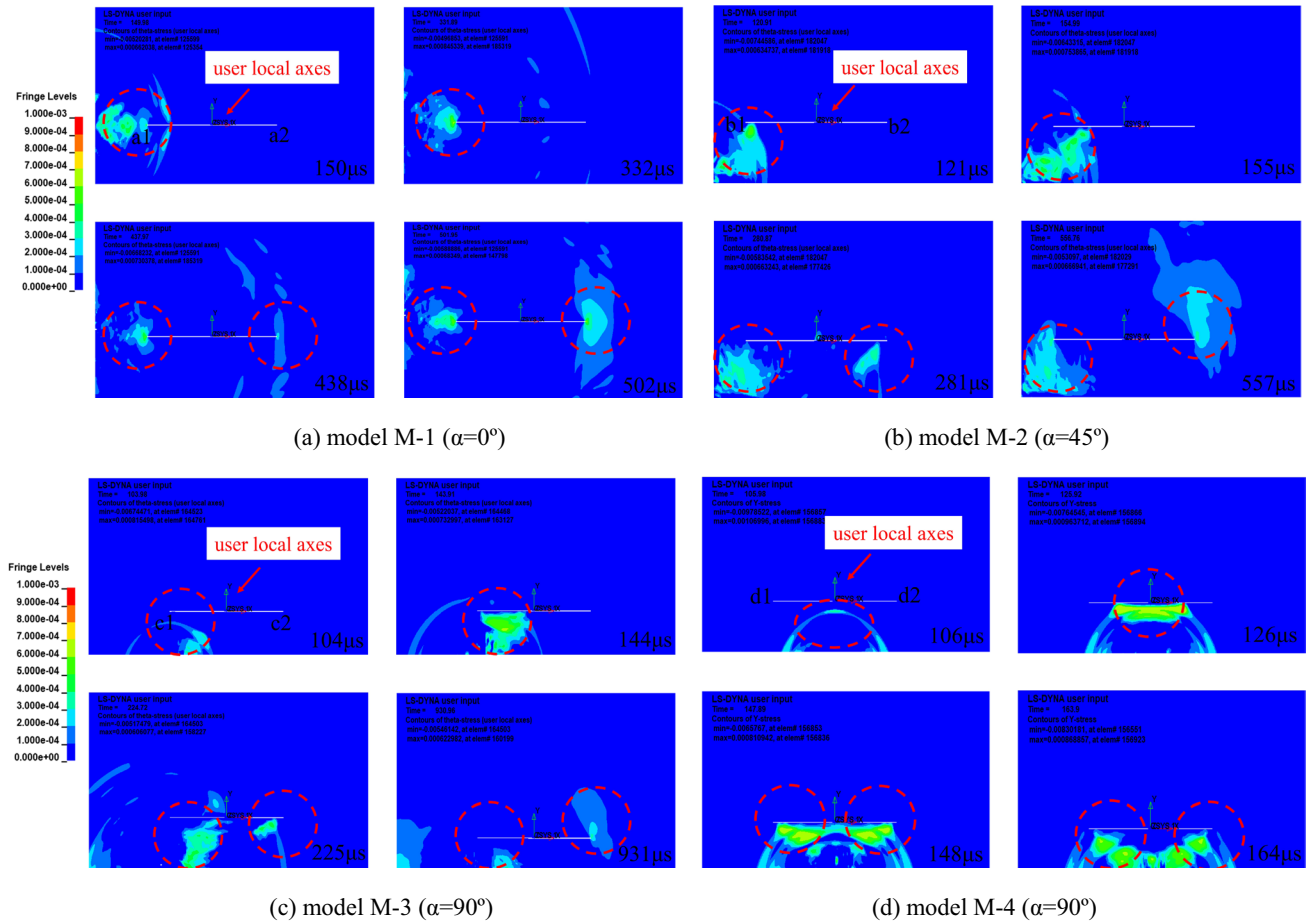

(a) model M-1 (α=0º) (b) model M-2 (α=45º)

(c) model M-3 (α=90º) (d) model M-4 (α=90º)

Fig. 18 Stress evolution with time at the crack tips

and τ_{xy} represent X-stress, Y-stress and shear stress; and θ represents the polar angle.

Figure 18a–d shows that the circumferential tensile stress changes with time near the crack tip when $\alpha = 0^{\circ}$, 45° and 90°; the circumferential tensile stress distribution indicates that the blasting stress waves induce stress concentration at the crack tip. And the evolution curves of circumferential tensile stress at crack tips captured in the four models are provided in Fig. 19a–d. From the sequence in Fig. 19, we note that the stress oscillates with time. In Fig. 18a, when $t = 150$ μs, the circumferential tensile stress near the crack tip A reaches a maximum, and tip A initiates at this time and gradually propagates to the left. Then, with further propagation of the stress wave, at $t = 438$ μs, the circumferential tensile stress near the crack tip B reaches a maximum, which results in that crack tip B initiates and gradually propagates to the right. Figure 18a and Fig. 19a also indicate that the stress distributions near the crack tips A and B are approximately symmetrical, the pre-existing crack propagates along the horizontal direction to both ends, respectively, and final crack path is roughly straight. Similarly, Fig. 18b–d can be analyzed, and there will not repeat it. In the meantime, it is also shown that, in Fig. 19b–d, the crack initiates when the circumferential tensile stress reaches a maximum. While Fig. 19b–d shows obviously different from Fig. 19a, that is not symmetrical; thus, crack propagation paths are curved. It is worth noting that, at $t = 106$ μs, a new crack appears at first below the midpoint of the pre-existing crack in Fig. 15d, and the circumferential tensile stress also reaches its maximum at this time, as shown in Fig. 18d. Additionally, there curves at the crack tips A and B in Fig. 19d almost coincide, indicating that almost same stress field at tips A and B is created when the pre-existing crack is symmetric with respect to the borehole, but only crack propagation path is not exactly the same as shown in Fig. 15d.

On the basis of the above analysis of the propagation of blasting stress waves with different incidence angles and crack behavior, the propagation characteristics of blasting-induced stress wave and dynamic behaviors of that interaction with the pre-existing crack are comprehensively reflected. Due to the different incident angle α, these mechanical properties and aging characteristics of blasting

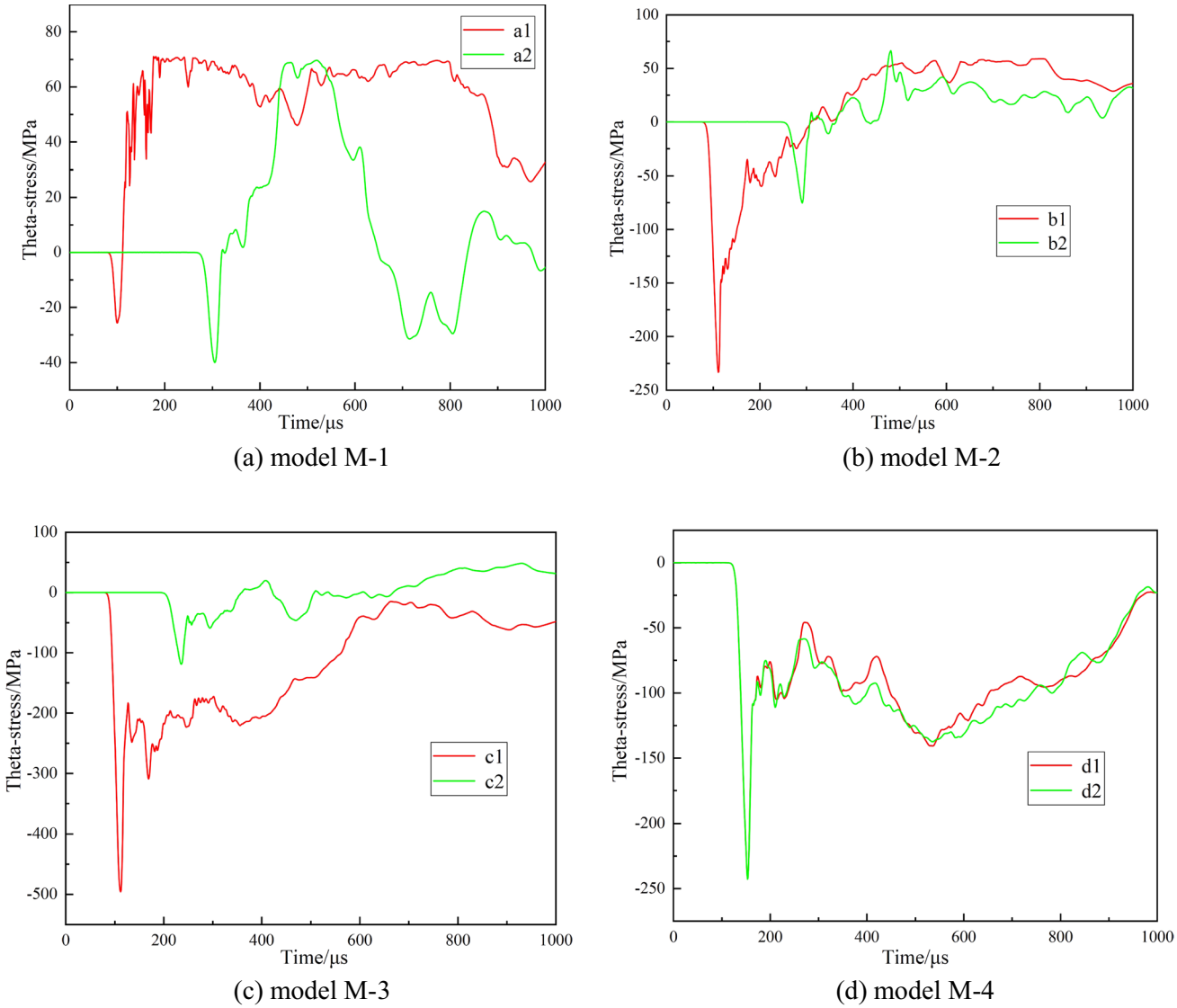

Fig. 19 Evolution curves of the circumferential tensile stress with time at the crack tips

stress wave cause the different dynamic behavior and failure modes of the models with the pre-existing crack at different stages. No blasting stress wave is transmitted to the upper surface of the pre-existing crack; the stress on it is caused by diffraction wave generated at the crack tips diffracting to the upper surface of the crack.

5 Conclusion

In this paper, the interaction between the blasting stress waves and pre-existing crack has been studied by finite element method combined with theoretical analysis, in which the influences of the incident angles of blasting stress waves on the wave propagation, crack initiation and propagation have been detailedly analyzed. The comparative analysis shows that numerical simulation agrees well with the experimental results and theoretical wavefront reconstruction, indicating that the numerical simulation used in this study can well characterize the interaction between the blasting stress waves and pre-existing crack. Actually, this is of great significance to the control and prediction of fracture and fragmentation of rock in actual blasting.

The incident angles of blasting-induced stress waves influence remarkably the propagation characteristics of waves at the pre-existing crack and model failure mode. The existence of cracks in rock leads to discontinuity of rock medium, hinders wave propagation and reduces its amplitude and restrains the formation and development of cracks around the borehole. Thus, the model damage is mainly

concentrated at the pre-existing crack ends, and around the borehole, no obvious damage occurs in other areas. In addition, reflected wave and diffraction wave cause stress concentration at the crack tip, which plays a dominant role in crack initiation and propagation. With the incident angle increasing, initiating time of crack tip B decreases, but the deflecting angle increases, and damage near the pre-existing crack is more serious.

In the end, it is worth mentioning that only the longitudinal wave radiating from the borehole is considered, while the shear wave is ignored due to the simplified plane strain. Besides, the incident angle of blasting stress wave discussed in this paper is one of the factors affecting the blasting effect. To more realistic description of the whole explosion progress, the more factors should be introduced in the future.

Acknowledgements This research was supported by the National Natural Science Foundation of China (No. 51974316) and the Fundamental Research Funds for Central Universities (Nos. 2022JCCXLJ01 and 2023ZKPYLJ04).

Funding This research was supported by the National Natural Science Foundation of China (No. 51974316) and the Fundamental Research Funds for Central Universities (Nos. 2022JCCXLJ01 and 2023ZKPYLJ04). Awards were granted to the author Liyun Yang.

Data Availability Data and material will be preserved and will be available upon request.

Code availability Software used is commercially available. If needed, authors can help readers in finding the companies providing software used in this work.

Declarations

Conflict of interest On behalf of all authors, the corresponding author states that there is no conflict of interest.

References

Bi CC (2018) Calibration of HJC constitutive parameters of Huashan granite and its blasting damage numerical simulation. Hefei University of Technology

Chen C, Yang RS, Xu P et al (2022) Experimental study on the interaction between oblique incident blast stress wave and static crack by dynamic photoelasticity. Opt Lasers Eng 148(3):106764

Chen PE, Sih GC (1977) Chapt. l and 3 of Elastodynamic Crack Problems. In: Mechanics of Fracture 4 (ed. by G.C. Sih), Noordhoj Int. Publ, Leyden

Dally JW (1980) An introduction to dynamic photoelasticity. Exp Mech 20(12):409–416

Dally JW, Fourney WL, Holloway DC (1975) Influence of containment of the bore hole pressures on explosive induced fracture, lnt. J. Rock Mech. Mix. Sci. Geomech. Abstr. 12:5–12

Fan LF, Zhou XF, Wu ZJ et al (2019) Investigation of stress wave induced cracking behavior of underground rock mass by the numerical manifold method. Tunnel Underground Space Technol 92:103032–103032

Gao XN, Wu YJ (2015) Numerical calculation of TNT explosion and its influencing factors. Chin J Explos Propell 38(3):32–39

Harris JG (1980) Diffraction by a crack of a cylindrical longitudinal pulse. J Appl Math Phys 31(3):367–383

Herakovich CT (2016) A concise introduction to elastic solids. Springer, Berlin

Hoop AT (1958) Representation theorems for the displacement in an elastic solid and their application to elastodynamic diffraction theory. PhD Thesis. Delft University of Technology, The Netherland

Hu R, Zhu ZM, Xie J et al (2015) Numerical study on crack propagation by using softening model under blasting. Adv Mater Sci Eng 2015:108580–108580

Jing L (2003) A review of techniques, advances and outstanding issues in numerical modelling for rock mechanics and rock engineering. Int J Rock Mech Min Sci 40(3):283–353

Jing L, Hudson JA (2002) Numerical methods in rock mechanics. Int J Rock Mech Min Sci 39(4):409–427

Lalegname A, Sändig AM (2011) Wave-crack interaction in finite elastic bodies. Int J Fract 172(2):131–149

Li JC, Ma GW (2010) Analysis of Blast Wave Interaction with a Rock Joint. Rock Mech Rock Eng 43(6):777–787

Li XB, Li CJ, Cao WZ et al (2018) Dynamic stress concentration and energy evolution of deep-buried tunnels under blasting loads. Int J Rock Mech Min Sci 104:131–146

Li Q, Xu WL, Wang K et al (2021) Study on the mechanical behavior of crack propagation effect at the end of defect under explosive load[J]. Int J Rock Mech Min Sci 138(3):104624

Qiu P, Yue ZW, Yang RS (2019) Mode I stress intensity factors measurements in PMMA by caustics method: A comparison between low and high loading rate conditions. Polym Testing 76:273–285

Qiu P, Yue ZW, Yang RS et al (2021) Modified mixed-mode caustics interpretation to study a running crack subjected to obliquely incident blast stress waves. Int J Impact Eng 150(3):103821

Rossmanith HP, Shukla A (1981a) Photoelastic investigation of stress wave diffraction about stationary crack-tips. J Mech Phys Solids 29(5–6):397–412

Rossmanith HP, Shukla A (1981b) Dynamic photoelastic investigation of interaction of stress waves with running cracks. Exp Mech 21(11):415–422

Saharan MR, Mitri HS, Jethwa JL (2006) Rock fracturing by explosive energy: review of state-of-the-art. Fragblast 10(1/2):61–81

Smith DG (1971) A Photoelastic Investigation of Stress-wave Loading of a Crack" SESA Spring Meeting 1971, Salt Lake City, Utah.

Theocaris PS, Katsamanis P (1978) Response of cracks to impact by caustics. Eng Fract Mech 10(2):197–210

Wang ZJ (2003) Experimental investigation on tamped and cavity decoupled explosion in rock-soil by mili-explosive charge. Changsha:National University of Defense Technology

Wang CY, Sun AY, Yang XY et al (2018) Numerical simulation of the interaction of laser-generated rayleigh waves with subsurface cracks. Appl Phys A 124(9):613

Woods RD (1969) A new tool for soil dynamics. J Soil Mech Found Div Asce, 94

Yang RS, Chen C, Yue ZW et al (2018) Dynamic photoelastic investigation of interaction of normal incidence blasting stress waves with running cracks. J China Coal Soc 43(3):638–645

Yang RS, Xu P, Chen C (2019) Interaction between blast stress waves and cracks. Explos Shock Waves 39(8):081102–081111

Yue ZW, Qiu P, Yang RS et al (2017) Stress analysis of the interaction of a running crack and blasting waves by caustics method. Eng Fract Mech 184:339–351

Yue ZW, Qiu P, Yang RS et al (2019) Experimental study on a Mach cone and trailing Rayleigh waves in a stress wave chasing running crack problem. Theor Appl Fract Mech 104:102371

Zhao J, Cai JG, Zhao XB et al (2003) Transmission of elastic P-waves across single fracture with nonlinear normal deformation behavior. Chin J Rock Mech Eng 22(1):9–17

Zhu ZH (1988) Dynamic photoelastic study of stress wave effect on crack propagation. J PLA Univ Sci Technol 04:78–84
Zhu ZH (1993) Dynamic photoelastic investigations of the effect of explosive stress waves on an extending-high speed crack. Explos Shock Waves 13(002):178–185